Applied Food Research 6 (2026) 101880

Contents lists available at ScienceDirect

Applied Food Research

journal homepage: www.elsevier.com/locate/afres

Modelling of chicken breast fillets for advanced poultry process automation

Matthias Vink [a,*], Hao Shi [a], Jovana Jovanova [a], Jan-Willem Kortlever [b], Dingena Schott [a]

[a] Department of Maritime and Transport Technology, Faculty of Mechanical Engineering, Delft University of Technology, Delft, 2628CD, The Netherlands
[b] Technisch Buro Kortlever B.V., Meerkerk, 4231DJ, The Netherlands

ARTICLE INFO

Keywords:
Bonded-particle
Bulk flow behaviour
DEM modelling
Food material modelling
Food processing equipment design
Meta-particle
Poultry handling
Soft tissue characterisation
Raw breast fillet

ABSTRACT

This study introduces a computational framework for modelling raw chicken breast fillets using the Discrete Element Method (DEM), aimed at providing a baseline efficient simulation model for large-scale poultry handling processes. A bonded multi-sphere meta-particle representation was developed and calibrated through mechanical testing of raw fillets. Compression experiments yielded a Young's modulus of approximately 48.6 kPa, which informed the stiffness properties of the DEM sub-particle assembly. Numerical Design of Experiments (DoEs) highlighted the need for an unbalanced ratio between normal and shear bond stiffness to ensure correct damping behaviour and preserve realistic flexibility. The framework was validated using a full-scale hopper–conveyor discharge experiment, demonstrating the model's ability to reproduce key physical behaviours such as large deformations, curling during discharge, and the transition between jammed and free-flow regimes. The simulation closely matched the measured discharge rate, with all chicken fillets discharged within 4 s at a 6 cm gate opening height. The proposed model required approximately 9 mins to simulate a 10-second industrial-scale process, underscoring the model's practical suitability for simulation-aided design and optimisation of poultry processing equipment.

1. Introduction

Global poultry consumption is on a consistent upward trajectory, driven by its cost-effectiveness, high nutritional profile, and the expanding variety of further-processed products (Sudheer, 2025; Yang et al., 2021). This sustained demand places significant pressure on processing facilities to increase throughput while maintaining strict quality and safety standards, such as assessment of chemical contaminants in beverages and the usage of antimicrobial edible coatings in poultry products (Naghashan et al., 2022; Shahvandari et al., 2021). Meeting these demands requires higher throughput and greater consistency, prompting a shift towards automation. However, the development of automated systems for handling poultry is hampered by the complex, non-linear mechanical properties of biological tissues. Traditional design cycles for such equipment rely heavily on trial-and-error prototyping, which is both costly and time-consuming.

Computer-Aided Design (CAD) with tissue modelling is one of the promising solutions to reduce this labour-intensive prototyping. Tissue modelling is critical across diverse sectors, ranging from biomechanics to food processing, as it facilitates a deeper understanding of specific tissue behaviours and their environmental interactions. Significant advancements have been achieved in modelling meat and tissue using Finite Element Analysis (FEA), a widely adopted method for simulating soft tissue (Freutel et al., 2014). In the context of food engineering, 3D FEA has been successfully validated for predicting environmental interactions, such as the cooling rates of meat products within industrial processing facilities (Cepeda et al., 2013). Beyond macroscopic environmental interactions, multiscale computational frameworks have been developed to investigate the fundamental mechanical properties of meat structure at varying levels of complexity (Spyrou, 2020). Furthermore, Mohammadi et al. (2024) employed FEA to model surgical interactions, while Verma and Pullela (2024) details several hyper- and viscoelastic FEA models – such as the Standard Linear Solid or Burgers models (Huang et al., 2011; Lin, 2024) – capable of replicating soft tissue behaviour under diverse loading scenarios.

However, while these models offer high accuracy for individual tissue components, they demand substantial computational resources and remain limited in scope and scale. Recent research continues to explore the potential of FEA for specialised applications, such as the texture development and structural design of plant-based meat analogues (Zhang & Zhu, 2025). Despite its utility in these specific contexts, the high computational burden makes FEA less suitable for large-scale industrial simulations. Recent efforts to mitigate this include hybrid models that combine rigid body transformations with localised FEA (Kim et al., 2017; Romero et al., 2020), as well as data-driven approaches that seek to bypass FEA during runtime via predictive algorithms (Agafonov & Zelnik-Manor, 2024). Nevertheless, hybrid models

* Corresponding author.
E-mail address: vinkmatthias@outlook.com (M. Vink).

https://doi.org/10.1016/j.afres.2026.101880
Received 13 August 2025; Received in revised form 6 February 2026; Accepted 11 March 2026
Available online 12 March 2026

Table 1
Dimensions of the modelled fillets. Each size is generated in both original and mirrored variations.

No.	Length (mm)	Width (mm)	Thickness (mm)
1	144	72	40
2	172	72	32
3	176	72	40

remain computationally expensive, and learning-based approaches are constrained by the necessity of vast, pre-existing experimental datasets, which are scarce in the poultry processes.

The primary challenge in industrial poultry processing is that it involves the dynamic handling of thousands of individual fillets. This environment is characterised by a high frequency of complex interactions, both among the fillets themselves and between the fillets and the processing machinery. FEA is not well-suited for such large-scale dynamic problems; the computational cost associated with multi-body contact detection and non-linear deformation at this scale is prohibitive (Mottet & Tempio, 2017). With global poultry demand expected to experience a substantial growth of over 120% in the coming decades (Alexandratos & Bruinsma, 2012; Mottet & Tempio, 2017), there is an urgent need for models that can facilitate the simulation-based design of automated solutions to save substantial costs in design and optimisation.

In the domain of particle-based systems, the Discrete Element Method (DEM) has emerged as a powerful alternative for simulating complex material dynamics (Cundall & Strack, 1979). Originally developed for the analysis of rock problems, DEM calculates forces on particles based on their properties and overlap at every timestep; resultant accelerations, velocities, and positions are then updated iteratively. It has proven effective in modelling realistic material behaviours and driving design breakthroughs across several industrial processes (Chen et al., 2019; Schott et al., 2021; Xu et al., 2023). Notably, DEM has been successfully employed to simulate and analyse the behaviour of flexible products, such as wheat straw (Schramm & Tekeste, 2022; Schramm et al., 2021; Shi et al., 2023), grapes and kiwis (Wu et al., 2022; Zu et al., 2025), demonstrating the method's capability to handle large numbers of interacting bodies. However, existing research on flexible object modelling has focused mainly on simple beam-shaped geometries. Research tackling more complex shapes has often yielded relatively rigid models that fail to replicate the high flexibility of chicken fillets (Li et al., 2022). Consequently, no modelling methods currently exist for simulating chicken fillets or their interactions with machinery, and the relevant engineering properties required for such a model remain largely unknown. This study aims to address this gap by investigating the extent to which DEM can be utilised to model the realistic individual and bulk behaviour of chicken fillets. Rather than developing an exhaustive high-fidelity framework, this work serves as a foundational proof of concept, utilising valid simplifying assumptions to establish a computationally efficient model. The primary objective is to qualitatively capture the essential mechanical behaviour of chicken fillets and simulate large-scale handling processes with reasonable computational overhead. By prioritising speed and behavioural accuracy over micro-physical detail, this model offers a viable tool for Computer-Aided Design (CAD) and simulation-aided optimisation (e.g., hopper and chute geometry in the handling process), representing a critical step towards the realisation of full automation in the poultry industry.

2. Methodology

The development of a computationally efficient DEM model for chicken fillets involves a multi-scale approach, transitioning from fundamental particle interactions to the simulation of complex bulk behaviour. This section details the modelling framework and the relevant experiments used to achieve the final chicken fillet model.

2.1. Contact model: Hertz-Mindlin with JKR

To simulate the interactions between fillets and processing equipment, the Hertz–Mindlin (Hertz, 1882; Mindlin, 1949; Mindlin & Deresiewicz, 1953) with Johnson–Kendall–Roberts (JKR) model (Johnson et al., 1971) was employed. The Hertz–Mindlin model calculates the normal force (F_n) based on the elastic deformation of the particles. The normal force is defined as:

$$F_n = \frac{4}{3} E^* \sqrt{R^*} \delta_n^{3/2} \tag{1}$$

Where δ_n is the normal overlap, and the equivalent Young's modulus (E^*) and equivalent radius (R^*) are derived from the properties of the two interacting bodies (1,2):

$$\frac{1}{E^*} = \frac{1-\nu_1^2}{E_1} + \frac{1-\nu_2^2}{E_2} \tag{2}$$

and equivalent radius R^*:

$$\frac{1}{R^*} = \frac{1}{R_1} + \frac{1}{R_2} \tag{3}$$

In this formulation, E represents the Young's modulus and ν the Poisson's ratio. To account for the adhesion characteristic of biological tissues, the JKR model modifies the normal force by incorporating the interfacial surface energy (γ). Under the JKR framework, the normal force F_{JKR} and the overlap δ_n are expressed in terms of the contact area radius (a) (Johnson et al., 1971):

$$F_{JKR} = \frac{4E^*}{3R^*} a^3 - 4\sqrt{\pi \gamma E^*}\ a^{3/2} \tag{4}$$

$$\delta_n = \frac{a^2}{R^*} - \sqrt{\frac{4\pi\gamma a}{E^*}} \tag{5}$$

The JKR model is highly relevant for chicken fillets as it accounts for the "pull-off" force required to separate adhering surfaces, e.g., sticking among the fillets and between fillets and handling equipment. The rolling friction was intentionally omitted from the contact model. While rolling friction is often used in DEM to compensate for the "rolling" of spherical particles, the irregular, non-spherical geometry of the whole fillet naturally resists rolling. By utilising a multi-sphere meta-particle approach, the bulk mechanical resistance and friction behaviour are governed by the macro-shape rather than an artificial rolling friction coefficient.

2.2. Chicken fillet: Bonded particle model

The primary challenge in representing a chicken fillet lies in its irregular shape and inherent flexibility. To achieve this, fillets were modelled as meta-particles–complex assemblies composed of 4 mm radius sub-particles. Six distinct mesh-based representations were developed to capture natural size variance (three sizes and their mirrored counterparts), as shown in Fig. 1, and their corresponding actual size variations are given in Table 1.

To replicate tissue flexibility, the Bonded Particle Model (BPM) (Potyondy & Cundall, 2004) was utilised to connect the sub-particles. To maximise the range of motion and prevent the model from becoming overly rigid, torque feedback within the bonds was disabled. The normal (δF_n) and tangential (δF_t) force increments per timestep within a bond are calculated as follows:

$$\delta F_n = \upsilon_n S_n \pi R_b^2 \delta_t \quad \text{and} \quad \delta F_t = \upsilon_t S_t \pi R_b^2 \delta_t \tag{6}$$

where υ_n and υ_t are the normal and tangential velocities of the particle, $S_{n,t}$ is the bond stiffnesses, R_b the particle radius multiplied by the bonded disk scale (set to 1.0 without any scaling) and δ_t is the timestep. Notably, these equations exclude damping terms. Instead, a specific strategy for energy dissipation using an unbalanced stiffness in normal and tangential directions was developed, which will be elaborated and discussed in the sensitivity section.

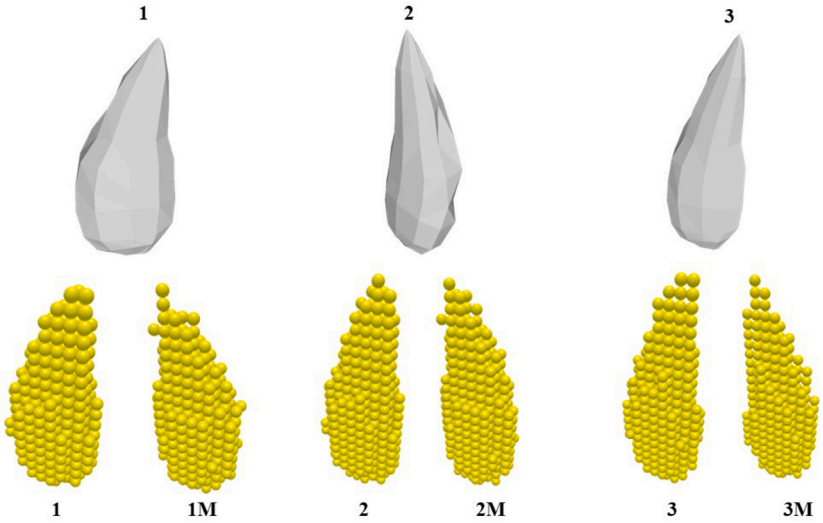

Fig. 1. Three chicken fillets shape variations and their corresponding generated bonded metaparticles. Each metaparticle is generated in two sub-variations: original and mirrored (marked with letter "M").

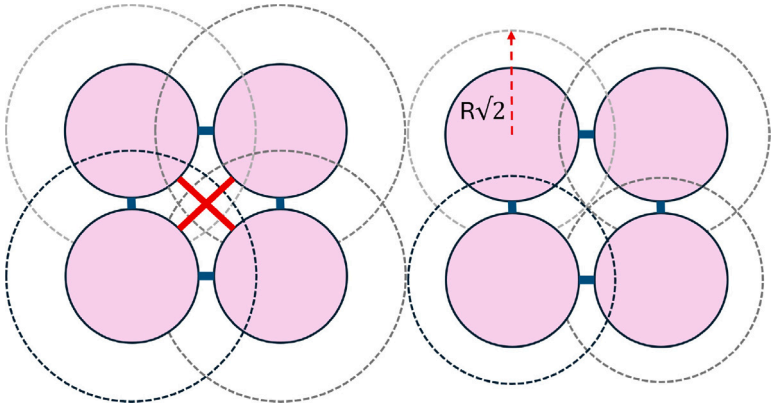

Fig. 2. Illustration showing (a) unwanted bonds forming a rigid truss structure in red and (b) the contact radius limit for preventing these undesired bonds forming.

To ensure the meta-particle remained intact under loading conditions, normal and shear strengths were set to a near-infinite value (1×10^{300} Pa), which prevents the bond from breaking due to the yielding of the maximum strength. A dual-particle-type system was implemented to enhance flexibility without sacrificing structural integrity, which is shown in Fig. 2. If a single particle type were used with an increased contact radius, a "stiff truss" structure would form due to the unwanted diagonal bonding (Fig. 2a). This limits the contact radius to $R\sqrt{2}$ without the formation of these diagonal bonds. By utilising two distinct particle types and only defining bonds between different types, the maximum contact radius can be effectively increased to $R\sqrt{3}$ without creating the undesirable diagonal stiffening bonds, as shown in Fig. 3. Note that although the bond strength is set to nearly infinite, the bonds can still break/fail if the distance between the two bonded particles exceeds the sum of the two contact radii, e.g., large tensile deformation that pulls one particle far away from its neighbouring bonded particle.

The numerical framework was implemented using the DEM software Altair EDEM^{TM} 2023. All simulations were executed on a standard workstation consisting of an NVIDIA RTX 3070 Ti GPU and a 12th-generation Intel i7 CPU. The scale of the final bulk fillets handling experiment involved the simultaneous simulation of 191 fillets, which comprised a total of over 41,000 sub-particles. Utilising GPU acceleration was critical to maintaining the computational efficiency, and the example computational cost of the case above is 9 mins GPU time for a 10-second real-life process that has an effective discharging throughput of 7.6 kg/s.

2.3. Model input parameters

The model parameters were established through a tripartite approach involving a review of existing literature, controlled laboratory experiments, and iterative calibration via sensitivity analyses. For the cases where specific input parameters were absent in the literature, the best available empirical alternatives were reviewed and utilised.

2.3.1. Material properties from literature

Initial mechanical properties were derived from benchmarks in soft tissue biomechanics. While specific data for chicken fillets is sparse, Choi and Zheng (2005) reported that the Young's modulus for general soft biological tissues typically ranges between 10–60 kPa (0.01–0.06 MPa) in indentation or low-strain-rate environments.

For the Poisson's ratio (ν), a value of 0.37 was assigned to the individual sub-particles. In the absence of specific literature for raw breast fillets, this value was adopted from Jahanbakhshian et al. (2017), who investigated the properties of chicken nugget crumbs at 7 °C. While crumbs represent a processed poultry derivative, they provide a reasonable approximation of the constituent tissue's elasticity under standard factory temperatures. It is important to emphasise that this

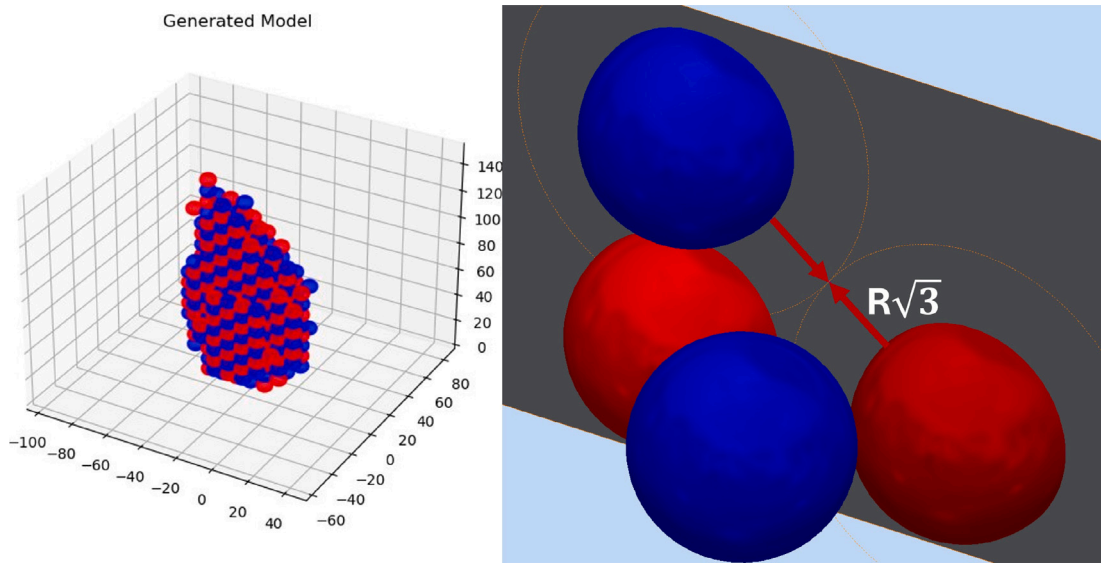

Fig. 3. The full model with 2 particle types (a), illustrating the increase in maximum contact radius (b).

ratio is defined at the sub-particle level (as in Fig. 1); the effective Poisson's ratio of the final meta-particle is an emergent property resulting from the collective interactions of the sub-particle assembly and the defining mechanical bonds.

To incorporate the inherent stickiness of the fillets, the Hertz–Mindlin contact model with JKRv2 was employed (Hertz, 1882; Johnson et al., 1971; Mindlin, 1949; Mindlin & Deresiewicz, 1953). While the precise interfacial surface energy (γ) of raw fillets is not explicitly defined, Silva et al. (2024) quantified the critical surface tension of chicken breasts at 54.56 mN/m (0.055 J/m^2), which is used as the baseline for the JKRv2 adhesion parameters. Due to the predominantly sliding nature of the fillets and their irregular geometry, rolling friction was omitted, and coefficients of restitution were minimised (0.0001) to replicate the substantial energy dissipation observed during physical handling.

2.3.2. Experiments using individual chicken fillet

To establish a validated foundation at the individual scale, a series of experiments was conducted to characterise the mechanical properties of a single chicken fillet, as shown in Fig. 4. These small-scale tests aim to verify the meta-particle's behaviour by quantifying its response to specific physical loads. By measuring these individual fillet behaviours through compression, bending, and sliding tests, we provide the empirical basis necessary to verify the model's performance before transitioning to the simulation of complex bulk-handling processes.

The initial phase of experimental calibration focused on the material level through a series of compression tests (Fig. 4a). Three $35 \times 35 \times 10$ mm samples were carefully extracted from a raw chicken fillet and subjected to compression using a Zwick/Roell compression tester equipped with an Xforce P load cell, reaching a maximum force of 20 N and a constant loading speed of 1 mm/min. The Young's modulus (E) was derived specifically from the linear region (within 3% strain) of the stress–strain curve recorded during the compression phase.

Subsequently, the external interaction between the fillets and the processing machinery was evaluated using an inclined plane sliding test (Fig. 4b). A stainless steel plate (SAE304) was gradually tilted until the fillet initiated a sliding motion, at which point the critical angle of inclination (α) was observed and recorded. To account for the variable conditions found in industrial processing facilities, these tests were performed with both dry and wet chicken fillets. This distinction allowed for an assessment of how surface moisture and the resulting adhesion influenced the critical sliding angle.

On a structural level, the internal bond stiffness parameters of the meta-particle were configured through a qualitative bending analysis, as illustrated in Fig. 4c & d. This experiment compared the deformation of a physical chicken fillet as it rolled off a conveyor ledge with the simulated behaviour of the bonded-particle assembly. By a numerical design of experiments (DoE), the bond model was calibrated to replicate the natural flexibility of raw fillets.

2.3.3. Sensitivity and model stability

Beyond providing flexibility at meta-particle/chicken fillet scale, the bond stiffness parameters significantly influence the model's numerical stability and damping characteristics upon impact. To define the operational limits of the framework and prevent numerical divergence during dynamic situations, a comprehensive sensitivity analysis was conducted. This analysis involved dropping a set of 90 modelled fillets (15 of each fillet representation as shown in Fig. 1) onto a horizontal surface under different conditions (impact speed, bond stiffness parameters and impact angles).

Performance was evaluated based on two primary metrics: the percentage of bonds remaining intact post-impact to assess structural integrity, and the time required for the system to dissipate total kinetic energy to evaluate damping efficiency. These simulations identified the stable parameter space necessary to replicate industrial interactions with high fidelity, ensuring the model remains robust against fracture or computational instability under realistic processing conditions. All final input parameters derived from these procedures are summarised in Table 2.

2.4. Experiments for bulk chicken fillets flow

After the determination of individual meta-particle properties, the framework was extended to evaluate the collective dynamics and bulk behaviour of the fillets. An experiment was designed using an industrial hopper positioned above a modular conveyor belt, replicating a standard configuration found in poultry processing lines. The hopper featured an adjustable front plate, or gate, through which the underlying conveyor belt extracted the fillets. The specific dimensions and geometric configuration of this experimental setup are detailed in Fig. 5.

The experimental procedure involved loading the hopper inner volume of 0.0407 m^3 with raw chicken fillets, which corresponds to a total mass of 38.21 kg. Once filled, the conveyor belt was activated and ran at a constant velocity of 15 m/min. The resulting outflow was observed

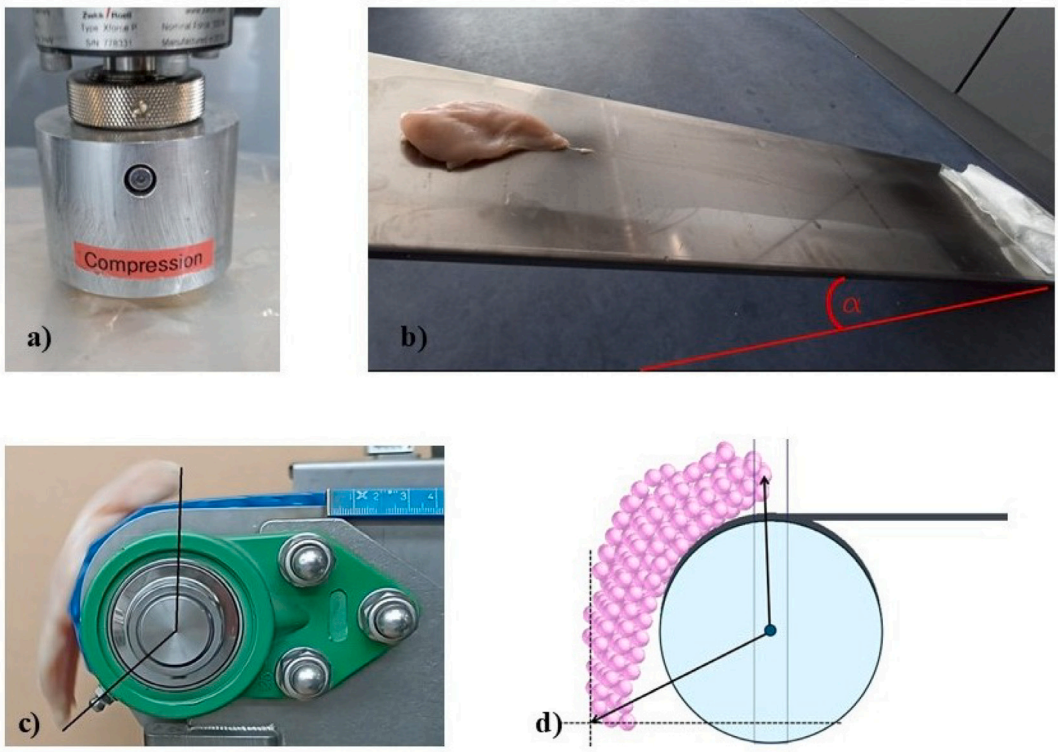

Fig. 4. Experiments for individual chicken fillet: (a) compression test; (b) sliding test; (c)&(d) bending test with its corresponding DEM model.

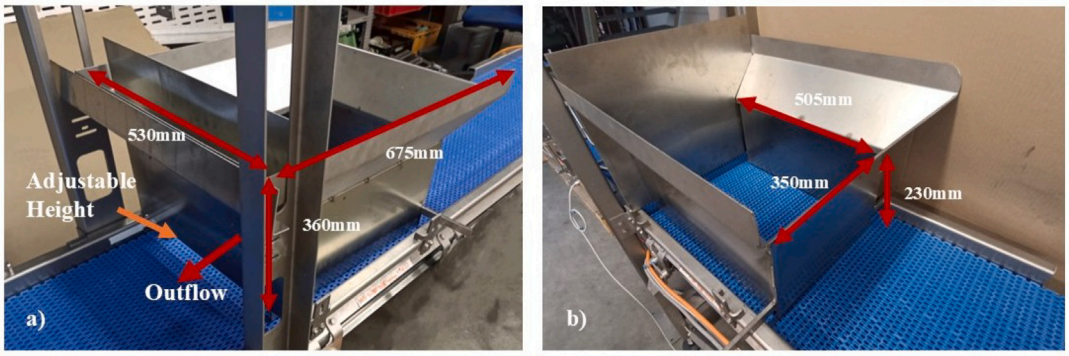

Fig. 5. The bulk experiment test setup: (a) front view, (b) back view. Two opening heights, 4.5 cm and 6 cm are tested via an adjustable opening plate.

to characterise the discharge behaviour and material flow patterns. To investigate the sensitivity of the flow to geometric constraints, the experiment was performed at two opening heights: 4 cm and 6.5 cm. Furthermore, to investigate common industrial practices where surface moisture is utilised to mitigate adhesion, water was added to the bulk fillets and tested at the two opening heights to examine the influence of lubrication on the flow dynamics. To provide a direct comparison between the empirical data and the numerical framework, the bulk experiment was also modelled in DEM by generating 191 fillet meta-particles in normal conditions. This setup allowed for a qualitative and quantitative evaluation of the simulation's ability to replicate real-world phenomena, such as flow and clogging at the opening.

3. Results and discussion

In this section, we present the experimental and numerical results used to calibrate and validate the chicken fillet model. We first analyse the material-level response through compression and individual behaviour (bending and sliding), followed by a sensitivity analysis of the bond parameters. Finally, we evaluate the bulk flow behaviour in an industrial hopper setup to demonstrate the model's validity and its potential for CAD applications.

3.1. Uniaxial compression of chicken breast fillet

In Fig. 6, we plot the stress–strain response of the raw chicken fillet samples obtained from the Zwick/Roell compression tests. The loading curves of three test samples are consistent with each other and reach almost identical final stress levels around 4 kPa, showing high repeatability of the compression behaviour. All three samples exhibit viscoelastic and strain stiffening behaviour. Therefore, the Young's modulus (E) was derived from the linear region of the compression loading curve (strain < 0.03), yielding an average value of 48.6 ± 1.64 kPa. While this is nearly an order of magnitude lower than the 0.37 MPa reported by Ko et al. (2023), it is important to note that the latter study utilised cooked chicken breast. The cooking process

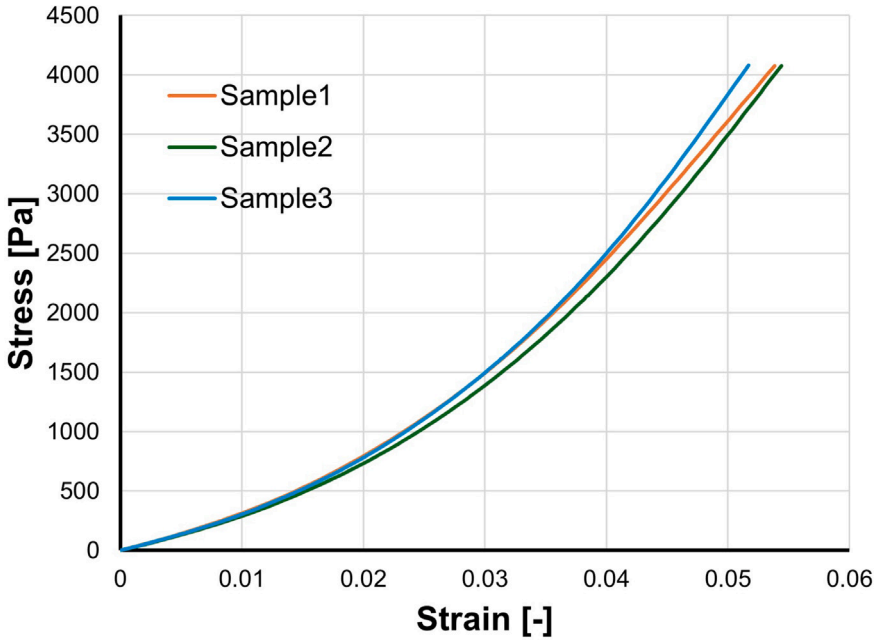

Fig. 6. The stress–strain curves resulting from the compression test.

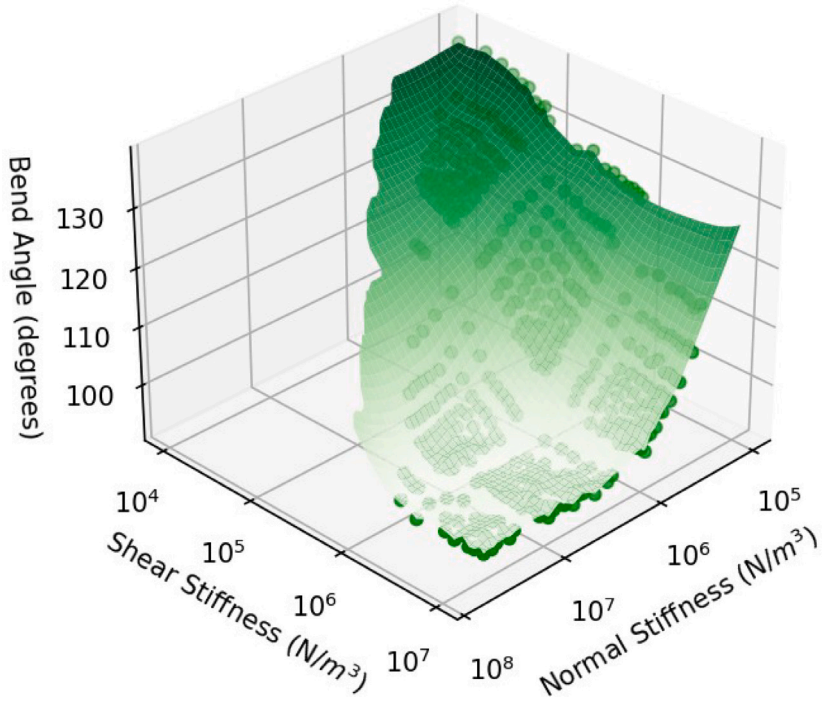

Fig. 7. Bend angles of the model for different stiffness combinations.

denatures proteins and reduces water content, significantly increasing the structural stiffness of the tissue. In contrast, our result aligns closely with the 10–60 kPa range reported by Choi and Zheng (2005) for raw, hydrated soft biological tissues under low-strain-rate conditions. This agreement confirms that a modulus of approximately 48.6 kPa is a representative input for the sub-particle properties in simulations of raw fillets and thus will be further used in all the simulations.

3.2. Bending and sliding behaviour

To calibrate the structural flexibility of the meta-particles, Fig. 7 illustrates the relationship between bond stiffness and the resulting bend angle. As anticipated, the bend angle has an inverse relationship with both normal and shear stiffnesses, i.e., a decrease in stiffness leads to an increase in the bend angle. Achieving the high flexibility measured in real fillets (angles > 120°) requires relatively low bond stiffness values. This confirms that the bonded-particle assembly is capable of replicating the high degree of flexibility characteristic of raw chicken fillet. However, the parameter space reveals a distinct region of numerical instability. Specifically, when the normal stiffness is high relative to the shear stiffness, the model becomes unstable regardless of the simulation timestep (tested down to 10^{-10} s). Conversely, a higher shear-to-normal stiffness ratio merely results in a greater frequency of bond fractures rather than total system divergence. This suggests that

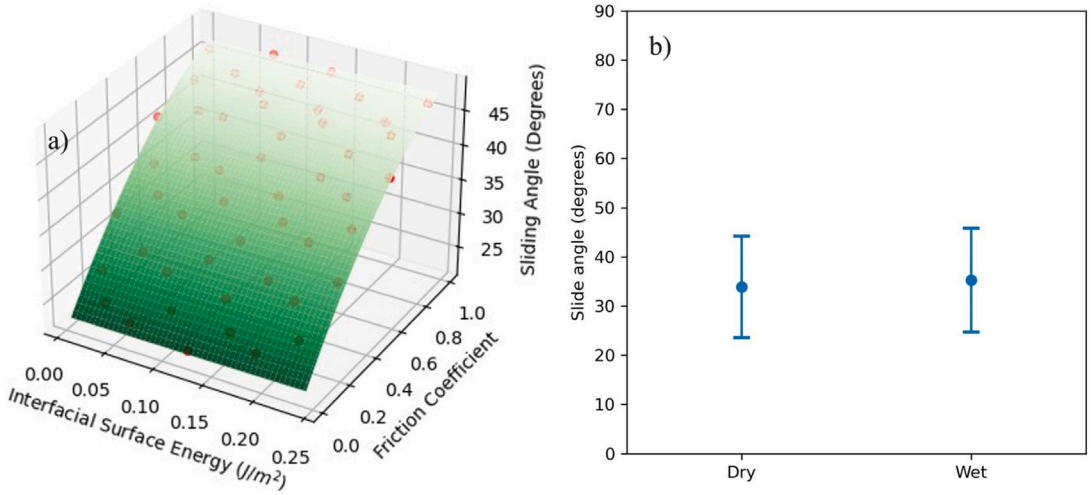

Fig. 8. (a) The sliding angle of the modelled fillet as a function of the interfacial surface energy and sliding friction coefficients between fillet particles and steel. (b) The influence of water on the sliding angle obtained from the sliding experiment using the real-life chicken fillets.

Table 2
Summary of the DEM model input parameters.

Bulk material:	Value	Unit
Poisson's ratio	0.37	–
Sub-particle Density	2200	kg/m^3
Meta-particle Density	940	kg/m^3
Young's modulus	48.6	kPa
Interactions, Fillets - Fillets		
Restitution	0.0001	–
Static Friction	0.1	–
Interactions, Fillets - Equipment		
Restitution	0.0001	–
Static Friction	0.5	–
BondingV2		
Normal stiffness per unit area	1e6	N/m^3
Tangential stiffness per unit area	6e5	N/m^3
Contact radius	6.928 ($\approx 4\sqrt{3}$)	mm
Normal/Shear strength	1e300	Pa
JKRv2, Fillets - Fillets/Equipment		
Interfacial surface energy	0.055	J/m^2
Simulator settings		
Timestep	5.75e−5	s

a state of equilibrium between normal and shear stiffness is required to maintain the structural integrity of the meta-particle during large deformations.

The sliding characteristics are analysed in Fig. 8a. From the numerical DoE, the coefficient of friction (μ) exhibits a strong linear correlation with the sliding angle. Surprisingly, the interfacial surface energy shows a negligible influence on the results. This aligns with our experimental observations, where immersing the fillets in water before slide testing did not significantly alter the sliding angle, as shown in Fig. 8b. These results suggest that for the scales and velocities considered here, the sliding behaviour is dominated by the friction coefficient rather than the adhesive force between the steel surface and the chicken fillet. Based on the fit between simulation and experimental data, a coefficient of friction of 0.5 was selected for the fillet-steel interaction.

3.3. Model stability and damping behaviour

In Fig. 9, we evaluate the damping behaviour using the settle time, which is the time taken for the whole chicken fillet to dampen 99% of its initial kinetic energy. The influences of bond stiffness in both normal and shear directions are examined here. The results reveal a "valley" shape, where low, unbalanced stiffness configurations result in the most efficient energy dissipation (minimum settle time). Balanced configurations (equal normal and shear stiffnesses) can take up to five times longer to dampen 99% of the kinetic energy after impact. Notably, these results demonstrate that realistic damping can be achieved through the intrinsic mechanics of the bonded assembly without the need for artificial global damping terms or extra damping terms to be added to the visco-elastic bond equations.

Next, we further evaluate the influence of the impact angles using the percentage of intact bonds post-impact, which is an essential indicator of the structural integrity of the meta-particle modelled. Fig. 10 shows all points in the numerical DoE space in which the impact angles were varied with respect to the principal axes of the chicken fillet (Pitch, Yaw and Roll). It is observed that the impact orientation significantly dictates bond survival; horizontal impacts distribute stress across a larger number of bonds, whereas vertical impacts on fewer sub-particles lead to localised stress concentrations and higher fracture rates.

In addition, the influence of impact velocity on model stability is illustrated in Fig. 11. The axes represent normal stiffness, shear stiffness, and impact velocity, while the colourbar denotes the percentage of intact bonds after impact. Each point corresponds to a single simulation, and those with more than 50% bond survival are highlighted to indicate regions of stable behaviour. The distribution of simulation points shows that lower impact velocities consistently lead to a higher percentage of intact bonds, as reflected by the predominance of blue tones at low velocities. In contrast, configurations that are stable under low-velocity impacts can become unstable when the velocity increases, suggesting that dynamic loading amplifies bond breakage even for comparatively stiff parameter combinations.

A mechanistic explanation for the observed failures can be drawn from the particle-level kinematics during impact. In many of the unstable configurations, particle pairs are displaced beyond a critical geometric limit, where the centre-to-centre separation exceeds the sum of their contact radii. Once this distance is surpassed, the bond is forced to break regardless of whether the internal stress in the bond has actually reached its yielding strength. Increasing the bond stiffness reduces the likelihood of such excessive separations and, in some regions of the parameter space, can even eliminate failure entirely, resulting in 100% intact bonds after impact. However, this comes at the cost of producing meta-particles that respond unrealistically rigidly. Excessive stiffness suppresses the highly deformable behaviour characteristic of real chicken fillet, thereby compromising the physical fidelity of the model.

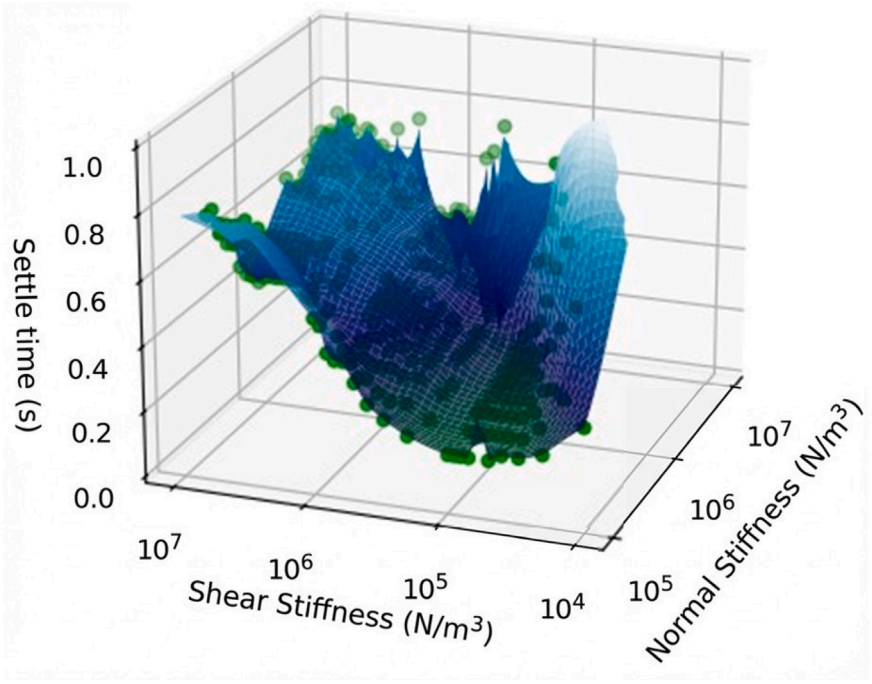

Fig. 9. The effect of bond stiffness on the settle time of the chicken fillet after its impact with the geometry.

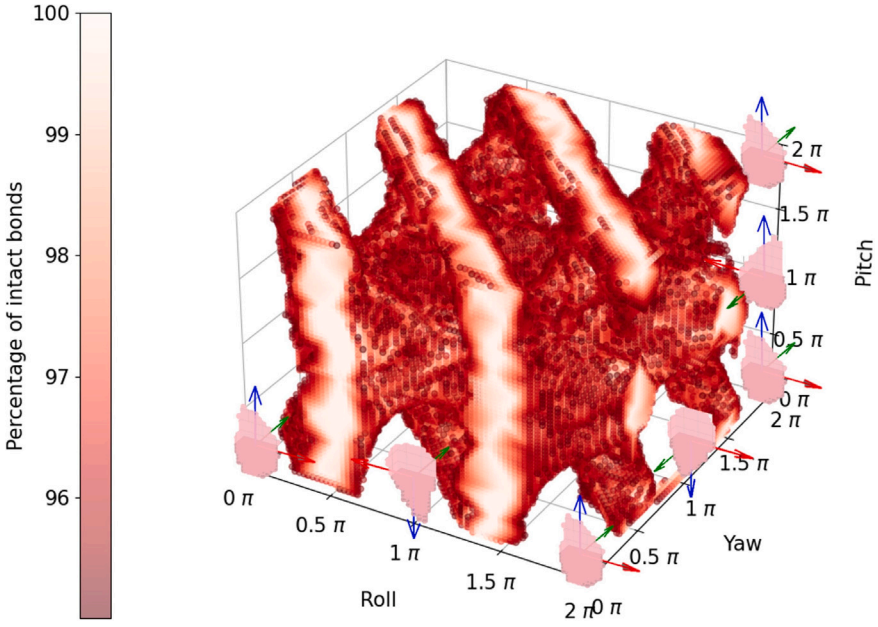

Fig. 10. The influence of impact angles on the stability (structural integrity) of the chicken fillet meta-particle after impact with different bond stiffnesses. Colourbar indicates the percentage ratio of the bonds before and after impact and is limited to above 95%.

The last sensitivity aspect falls onto the size scaling of the meta-particles (sub-particles), as it directly correlates to the total number of meta-particles, thus the computational cost of the simulation. Scaling the meta-particles had a pronounced effect on the model's stability, as shown in Fig. 12. At the smallest scale 1, the system exhibits a sharp transient: the settle time drops from 0.78 s to approximately 0.05 s, while the percentage of intact bond is very low (<5%). As the scale increases towards 2, the bond-survival fraction rises steeply and then plateaus near 100%; beyond this point, size scaling showed almost no influence on the bond integrity. In contrast, the settle time grows monotonically with scale from approximately 0.2 s to 0.5 s at scale 10 (with small oscillations).

The strong scale dependence arises because the contact radius, bond radius, normal and tangential stiffness (the values set per unit area stay constant) all increase with particle size (cf. Eq. (6)), so uniformly scaling up the size of the meta-particles (and sub-particles) raises the effective stiffness of the bond network. This stiffening suppresses subparticle detachments. In contrast, at the smallest scale, sub-particles are more readily displaced beyond the critical separation (center-to-center distance exceeding the sum of contact radii), forcing bonds to fail geometrically even when stresses remain below the yielding threshold/maximum strength; the consequence is the low percentage of intact bonds. The gradual increase in the settle time with scale is consistent with the damping behaviour observed earlier (Fig. 9):

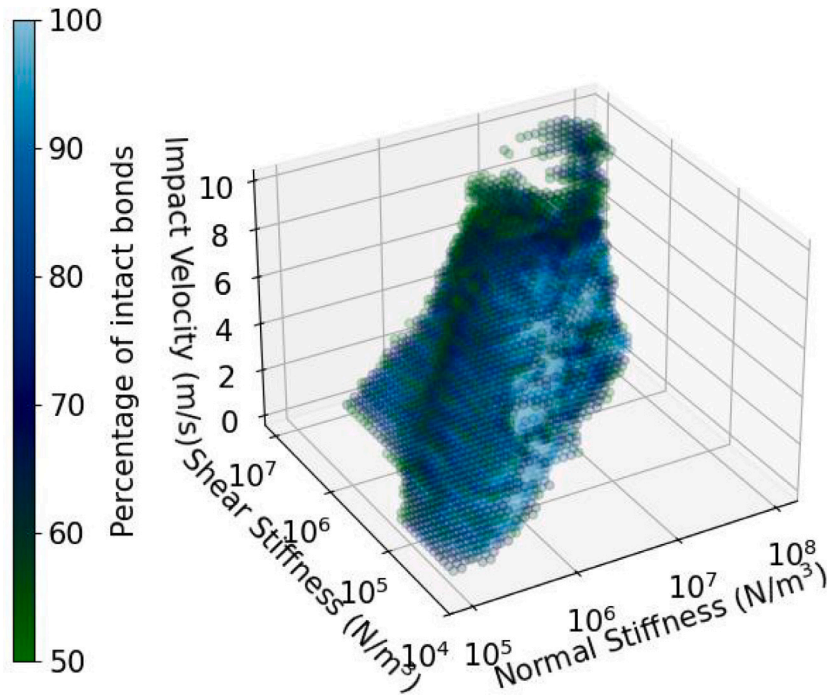

Fig. 11. The influence of impact velocity on the stability of the chicken fillet meta-particle after impact with different bond stiffnesses.

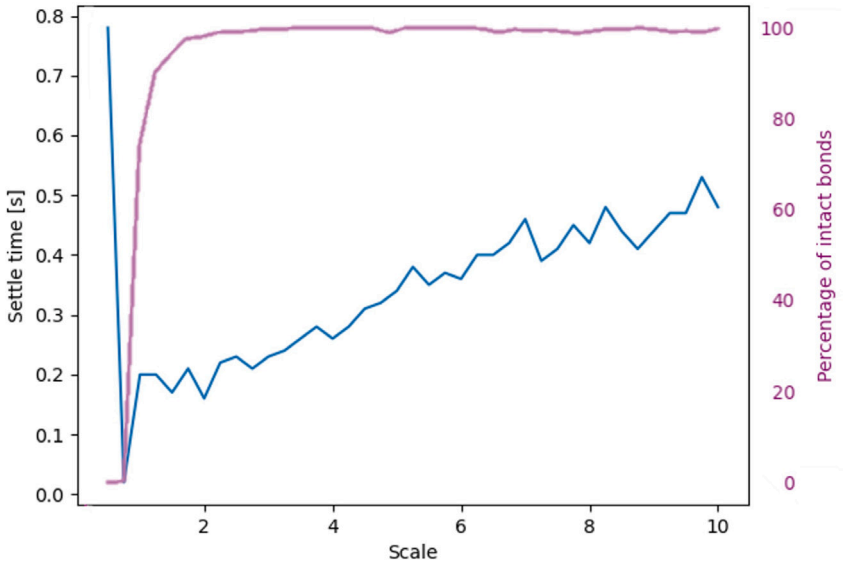

Fig. 12. The influence of particle size scale (0.25x - 10x) on model stability and its damping behaviour.

higher, well-balanced stiffness leads to slower energy dissipation, so the system takes longer to settle despite being mechanically stable. Practically, these results highlight a trade-off. Increasing scale value/bond stiffness can eliminate detachment-induced bond loss, but it also produces longer damped responses and over-rigid meta-particles that no longer capture the flexible character of the chicken-fillet. Selecting the balanced scales and corresponding stiffnesses just above the stability threshold (where percentage of intact bonds is 100% yet settle times remain moderate, e.g., scaling 1x with 4 mm subparticles) appears to offer the best balance between numerical robustness and physical realism.

Table 3
Chicken fillets flow behaviour in bulk experiments.

Opening height	Normal	With water
4.5 cm	Inconsistent flow	No flow
6 cm	Constant flow	Inconsistent flow

3.4. Validation of bulk flow behaviour

To evaluate the numerical framework's performance at an industrial scale, we compare the bulk discharge characteristics of the DEM model against physical experimental data through both qualitative comparison and quantitative mass flow measurements. In Table 3, we

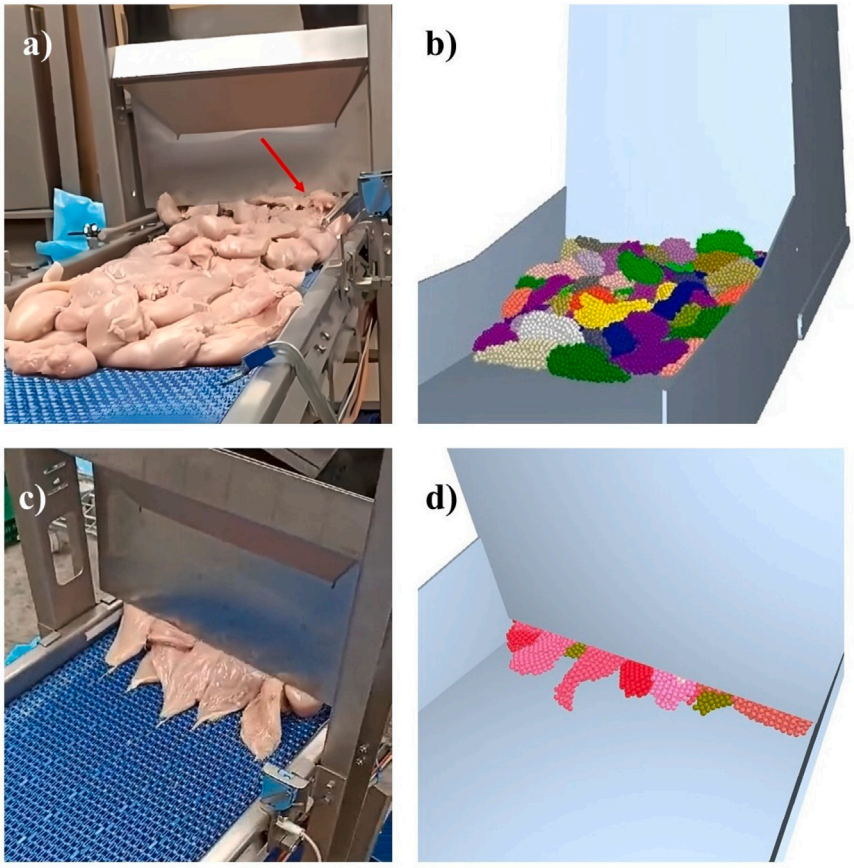

Fig. 13. Comparison between the bulk chicken fillets experiments and simulations: (a) normal chicken fillets with 6 cm opening height, (b) simulated flow behaviour with 6 cm opening height, (c) normal chicken fillets with 4.5 cm opening height, (d) simulated flow behaviour with 4.5 cm opening height.

summarise the discharge behaviour based on the opening height and the presence of surface moisture, identifying three distinct regimes: *constant flow*, *inconsistent flow*, and *no flow* (clogging). At an opening height of 4.5 cm, the normal fillets exhibit an inconsistent flow characterised by intermittent bridging across the hopper opening. When water is added to the bulk, this progresses to a total stoppage of flow. Physically, this transition suggests that the surface moisture enhances the adhesive forces between fillets, effectively reinforcing the internal stability of the packing of the fillets. Conversely, at an opening height of 6 cm, the normal fillets showed a steady and smooth flow. However, the wet fillets in this configuration again induce an inconsistent flow regime. This behaviour is likely attributed to a dual mechanism: the increased clumping due to moisture-induced adhesion and loss of traction between the wet fillets and the conveyor belt.

The visual fidelity of these interactions is further illustrated in Fig. 13, in which the flow behaviour at two opening heights was compared with the simulations for normal fillets. The DEM model accurately replicates the physical thresholds observed in the experiments, capturing the transition from a continuous discharge at the large opening height (Fig. 13a & b) to a jammed state at a small opening height (Fig. 13c & d). Furthermore, the bulk experiments revealed that as the fillets exit the hopper, they exhibit a characteristic "curling" and "draping" behaviour. The DEM model also captures this phenomenon, as the calibrated bond stiffness combination (high normal, low shear) allows the meta-particles to deform easily under their own weight. This qualitative agreement confirms that the individual-scale calibration of the meta-particles correctly translates to realistic collective dynamics in a bulk handling scenario.

For a more rigorous quantitative validation, we plot the mass flow rate of normal fillets using 6 cm opening height for both the experimental and DEM simulation in Fig. 14. In the experiment, around 33.2 kg of fillets were fully discharged from the hopper (exit the 6 cm opening) within 4 s. In simulation, the cumulative mass curve exhibits a linear increase trend with time and agrees well with the experimental measurement (around 7% error), indicating the validity of the DEM model and confirming the model's ability to predict industrial-scale chicken fillet handling behaviour.

The computational efficiency of this framework is a key highlight for industrial adoption. Utilising GPU acceleration on a standard workstation, the 10 s (the initial 4 s generation part was omitted in Fig. 14) of the bulk hopper discharge experiment was simulated in approximately 9 min. This performance represents a critical threshold for industrial application, as it allows for multiple large-scale design iterations to be conducted daily. This high computational throughput, combined with the observed physical accuracy, positions this DEM framework as the first step towards a viable and valuable tool for the development of new chicken fillet processing machinery, allowing engineers to refine concept designs and solutions while significantly reducing the expensive physical prototyping.

4. Conclusion and outlook

This study presents a novel numerical framework for simulating raw chicken fillets using the Discrete Element Method (DEM). A multi-sphere, bonded meta-particle formulation was developed to bridge the gap between tissue-scale mechanics and industrial-scale bulk handling. After calibration against compression, bending, and sliding experiments, the model was shown to reproduce key characteristics of poultry tissue, including its pronounced compliance and stochastic deformation response. The framework was further validated through qualitative assessments of flow regimes and quantitative measurements of mass

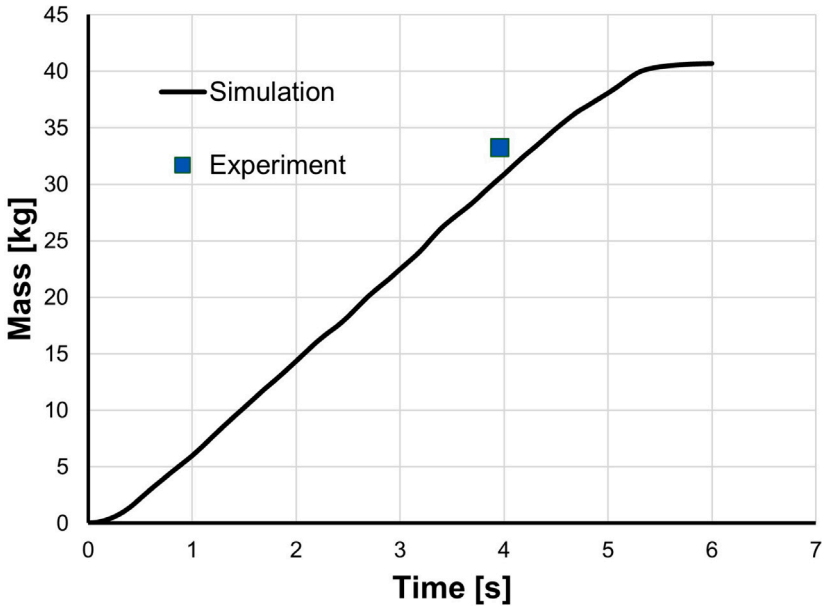

Fig. 14. Mass flow through the opening in the bulk chicken fillet experiment and simulation with 6 cm opening height.

flow rate, demonstrating its suitability as a virtual test environment for food-processing automation and equipment design.

A central contribution of this work is the systematic modelling method that enables the transition from a single sub-sphere description to a calibrated, application-ready bonded meta-particle. Rather than treating the meta-particle as an ad hoc construct, we established a reproducible process that: (i) defines the particle discretisation and bond topology, (ii) links bond and contact parameters to experimentally observable responses, and (iii) verifies the resulting material behaviour across multiple mechanical tests. This workflow provides a practical blueprint for constructing DEM representations of highly deformable biological materials.

Despite these advances, several limitations remain that also define clear directions for future work. While GPU acceleration enables high mass flow fillet discharge simulations, achieving true real-time performance for industrial-scale scenarios – particularly those requiring extensive optimisation campaigns – remains an important development goal and will be addressed through further model developments. A more fundamental limitation arises from the current bonding formulation, which can lead to separation-driven bond loss and numerical instabilities under extreme loading conditions, highly non-uniform impacts, or strongly unbalanced stiffness parameters. Mitigating these effects currently requires increased stiffness, improving robustness at the expense of physical realism by yielding overly rigid meta-particles that no longer capture the compliant behaviour of real chicken fillets. Addressing this coupled limitation motivates the development of an enhanced bonding formulation that remains stable over larger effective contact radii and wider deformation ranges. Finally, the framework can be further integrated into a numerical Design of Experiments (DoE) to systematically explore material parameters and equipment designs, enabling data-driven optimisation of automated poultry handling with improved throughput and reliability.

CRediT authorship contribution statement

Matthias Vink: Writing – review & editing, Writing – original draft, Visualization, Validation, Software, Resources, Project administration, Methodology, Investigation, Formal analysis, Data curation, Conceptualization. **Hao Shi:** Conceptualization, Formal analysis, Methodology, Visualization, Writing – review & editing. **Jovana Jovanova:** Writing – review & editing, Supervision. **Jan-Willem Kortlever:** Writing – review & editing, Supervision. **Dingena Schott:** Writing – review & editing, Supervision.

Ethics statement

This study did not involve any experiments on live animals or human participants. All chicken fillets used in the experiments were aquired from a commercial supplier.

Declaration of Generative AI and AI-assisted technologies in the writing process

During the preparation of this work the author(s) used Microsoft Copilot in order to improve the quality of the text. After using this tool/service, the authors reviewed and edited the content as needed and take full responsibility for the content of the published article.

Declaration of competing interest

The authors declare the following financial interests/personal relationships which may be considered as potential competing interests: Matthias Vink reports financial support and equipment, drugs, or supplies were provided by Technisch Buro Kortlever B.V. Reports a relationship with that includes: Has patent pending. If there are other authors, they declare that they have no known competing financial interests or personal relationships that could have appeared to influence the work reported in this paper.

Acknowledgements

The authors acknowledge Technisch Buro Korlever B.V. for supporting the experimental materials with associated costs and Delft University of Technology for supporting the modelling software. This research was carried out without any specific grant from funding agencies in the public, commercial, or not-for-profit sectors.

Appendix A. Supplementary data

Supplementary material related to this article can be found online at https://doi.org/10.1016/j.afres.2026.101880.

Data availability

Data will be made available on request.

References

Agafonov, A., & Zelnik-Manor, L. (2024). STMPL: Human soft-tissue simulation. arXiv preprint arXiv:2403.08344.

Alexandratos, N., & Bruinsma, J. (2012). World agriculture towards 2030/2050: the 2012 revision. *Research in Agricultural and Applied Economics*.

Cepeda, J., Weller, C., Thippareddi, H., Negahban, M., & Subbiah, J. (2013). Modeling cooling of ready-to-eat meats by 3D finite element analysis: validation in meat processing facilities. *Journal of Food Engineering*, *116*(2), 450–461.

Chen, G., Lodewijks, G., & Schott, D. L. (2019). Numerical prediction on abrasive wear reduction of bulk solids handling equipment using bionic design. *Particulate Science and Technology*.

Choi, A., & Zheng, Y. P. (2005). Estimation of Young's modulus and Poisson's ratio of soft tissue from indentation using two different-sized indentors: finite element analysis of the finite deformation effect. *Medical & Biological Engineering & Computing*, *43*(2), 258–264.

Cundall, P. A., & Strack, O. D. (1979). A discrete numerical model for granular assemblies. *Geotechnique*, *29*(1), 47–65.

Freutel, M., Schmidt, H., Dürselen, L., Ignatius, A., & Galbusera, F. (2014). Finite element modeling of soft tissues: material models, tissue interaction and challenges. *Clinical Biomechanics*, *29*(4), 363–372.

Hertz, H. (1882). Ueber die berührung fester elastischer körper.. *Journal Für Die Reine Und Angewandte Mathematik*, *93*, 156–171.

Huang, C.-C., Wei, M.-K., & Lee, S. (2011). Transient and steady-state nanoindentation creep of polymeric materials. *International Journal of Plasticity*, *27*(7), 1093–1102.

Jahanbakhshian, N., Hamdami, N., & Shahedi, M. (2017). Measurement and prediction of the mechanical properties of a two-component food during freezing. *International Journal of Food Properties*, *20*(sup3), S3088–S3095.

Johnson, K. L., Kendall, K., & Roberts, A. (1971). Surface energy and the contact of elastic solids. *Proceedings of the Royal Society of London, Series A (Mathematical and Physical Sciences)*, *324*(1558), 301–313.

Kim, M., Pons-Moll, G., Pujades, S., Bang, S., Kim, J., Black, M. J., & Lee, S.-H. (2017). Data-driven physics for human soft tissue animation. *ACM Transactions on Graphics*, *36*(4), 1–12.

Ko, C., Davies, A., & Auty, M. (2023). Putting meat to the test: Imaging and mechanical testing used to understand the properties of meat alternatives and how they mimic our typical meat sensory experience. *Microscopy Today*, *31*(2), 21–25.

Li, X., Du, Y., Liu, L., Mao, E., Wu, J., Zhang, Y., & Guo, D. (2022). A rapid prototyping method for crop models using the discrete element method. *Computers and Electronics in Agriculture*, *203*, 107451.

Lin, C.-Y. (2024). Rethinking and researching the physical meaning of the standard linear solid model in viscoelasticity. *Mechanics of Advanced Materials and Structures*, *31*(11), 2370–2385.

Mindlin, R. (1949). Compliance of elastic bodies in contact. *Journal of Applied Mechanics*, *16*(3), 259–268.

Mindlin, R., & Deresiewicz, H. (1953). Elastic spheres in contact under varying oblique forces. *Journal of Applied Mechanics*, *20*(3), 327–344.

Mohammadi, H., Ebrahimian, A., & Maftoon, N. (2024). Finite-element modelling of needle-tissue interactions. *Archives of Computational Methods in Engineering*, *31*(3), 1363–1404.

Mottet, A., & Tempio, G. (2017). Global poultry production: current state and future outlook and challenges. *World's Poultry Science Journal*, *73*(2), 245–256.

Naghashan, M., Kargarghomsheh, P., Nazari, R. R., Mehraie, A., Tooryan, F., & Shariatifar, N. (2022). Polycyclic aromatic hydrocarbons (PAHs) in fruit juice samples: a health risk assessment study. *Environmental Science and Pollution Research*, PREPRINT (Version 1).

Potyondy, D. O., & Cundall, P. A. (2004). A bonded-particle model for rock. *International Journal of Rock Mechanics and Mining Sciences*, *41*(8), 1329–1364.

Romero, C., Otaduy, M. A., Casas, D., & Perez, J. (2020). Modeling and estimation of nonlinear skin mechanics for animated avatars. In *Computer graphics forum: Vol. 39*, (2), (pp. 77–88). Wiley Online Library.

Schott, D., Mohajeri, J., Jovanova, J., Lommen, S., & de Kluijver, W. (2021). Design framework for DEM-supported prototyping of grabs including full-scale validation. *Journal of Terramechanics*, *96*, 29–43.

Schramm, M., & Tekeste, M. Z. (2022). Wheat straw direct shear simulation using discrete element method of fibrous bonded model. *Biosystems Engineering*, *213*, 1–12.

Schramm, M. W., Tekeste, M. Z., & Steward, B. L. (2021). Simulation of uniaxial compression for flexible fibers of wheat straw using the discrete element method. *Transactions of the ASABE*, *64*(6), 2025–2034.

Shahvandari, F., Khaniki, G. J., Shariatifar, N., Mahmoudzadeh, M., Sani, M. A., Alikord, M., Nabizadeh, R., & Kamkar, A. (2021). Chitosan/cumin (cuminum cyminum l.) essential oil edible biodegradable coating: its effect on microbial, physical and sensory properties of chicken meat during referigeration.. *Carpathian Journal of Food Science & Technology*, *13*(1).

Shi, Y., Jiang, Y., Wang, X., Thuy, N. T. D., & Yu, H. (2023). A mechanical model of single wheat straw with failure characteristics based on discrete element method. *Biosystems Engineering*, *230*, 1–15.

Silva, J. M. d., da Silva, E. M. C., de Matos, J. A., de Alcantara, L. O., & de Souza, B. W. S. (2024). The wettability of carrageenan-based edible coatings on chicken breasts. *Revista Ciência Agronômica*, *55*, e20217827.

Spyrou, L. (2020). A computational multiscale modeling framework for investigating the mechanical properties of meat. *Food Structure*, *26*, 100161.

Sudheer, K. (2025). Trends in poultry and egg-based foods. *Trends in Animal-Based Foods*, 271–289.

Verma, N., & Pullela, M. (2024). Material models for finite element analysis of soft tissues. In *Microbiology-2.0 update for a sustainable future* (pp. 427–450). Springer.

Wu, Z., Li, G., Yang, R., Fu, L., Li, R., & Wang, S. (2022). Coefficient of restitution of kiwifruit without external interference. *Journal of Food Engineering*, *327*, 111060.

Xu, C., Xu, F., Tang, H., & Wang, J. (2023). Determination of characteristics and establishment of discrete element model for whole rice plant. *Agronomy*, *13*(8), 2098.

Yang, Y., Wang, W., Zhuang, H., Yoon, S.-C., Bowker, B., Jiang, H., & Pang, B. (2021). Evaluation of broiler breast fillets with the woody breast condition using expressible fluid measurement combined with deep learning algorithm. *Journal of Food Engineering*, *288*, 110133.

Zhang, J., & Zhu, H. (2025). Finite element analysis as a promising approach for texture development of plant-based meat analogs. *Physics of Fluids*, *37*(3).

Zu, H., He, K., Liu, W., Liu, J., Song, Z., & Su, Y. (2025). Interaction properties of wine grapes: DEM analysis and experimental investigation. *Journal of Food Engineering*, *387*, 112347.